Unfolding of wave-arrival singularities in the elastodynamic Green's functions of anisotropic solids under weak spatial dispersion

A. G. Every
School of Physics, University of the Witwatersrand, PO WITS 2050, Johannesburg, South Africa

J. D. Kaplunov
Department of Mathematical Sciences, Brunel University, Uxbridge, Middelsex, UB8 3PH, United Kingdom

G. A. Rogerson
Department of Mathematics, Keele University, Staffordshire ST5 5BG, United Kingdom

(Received 13 June 2006; revised manuscript received 5 September 2006; published 17 November 2006)

In this paper we examine the effects on transient wave propagation of weak spatial dispersion, i.e., the first onset of dispersion as the acoustic wavelength approaches the natural scale of length of a medium. In centrosymmetric solids, and also away from acoustic axes in noncentrosymmetric crystals, this takes the form of a correction to the phase velocity which is quadratic in the wave vector **k**. Our analysis is developed for centrosymmetric solids for which weak spatial dispersion expresses itself through the presence of fourth order spatial derivatives of the displacement field in the wave equation. We examine the effect that spatial dispersion has on wave-arrival singularities in the elastodynamic Green's functions of anisotropic solids. These are singular features that propagate at the group velocities in each direction, and are interpreted on the basis of the stationary phase approximation. The focus of this paper is on wave arrivals associated with elliptic and hyperbolic points on the acoustic slowness surface. In the response to a suddenly applied point force, the wave arrival pertaining to an elliptical point takes the form of a step function, or where symmetry intervenes, a ramp function. The wave arrival for a hyperbolic point takes the form of a logarithmic singularity, or where symmetry intervenes, a softer logarithmic singularity. We report how, under the influence of weak spatial dispersion, these arrivals unfold into wave trains known as quasiarrivals, which conform to integral expressions involving the Airy function. For positive dispersion, i.e., the more common situation of downward curving dispersion relation, $\omega(\mathbf{k})$, the ripples of the wave train follow the arrival, whereas for negative dispersion they precede the arrival. The results presented here are of relevance in the broad context of transient acoustic waves in any situation where the characteristic wavelength approaches the natural scale of length of the medium, whether that be the interatomic spacing in a crystal, the repeat distance in a layered solid, or whatever. They are expected to be of particular interest in the topical field of picosecond laser ultrasonics.

DOI: 10.1103/PhysRevB.74.184307 PACS number(s): 62.30.+d, 62.65.+k, 43.35.+d

I. INTRODUCTION

The most striking feature of time domain elastodynamic Green's functions of solids is the wave-arrival singularities they contain.[1–4] In an anisotropic solid, these travel at the acoustic group velocities in each direction, and take on various analytic forms, such as the delta, step, and ramp functions and logarithmic and power law singularities.[4] Much of the acoustic energy radiated by a localized event, such as an impulsive or suddenly applied point force, is concentrated at these arrivals, and in the far field, they are essentially all that survives. Dispersion has the effect of rounding wave-arrival singularities, and spreading them out into wave trains known as quasiarrivals.[5–8] The focus of this paper is on the effect on wave arrivals of the first onset of spatial dispersion, i.e., the variation of the wave speed as the wavelength, λ, approaches the natural length scale, l, of the medium. This length scale might, for example, correspond to the lattice constant or range of interatomic forces in a crystal, or the repeat distance in a layered or fibrous solid. In centrosymmetric solids, weak spatial dispersion expresses itself as a correction to the phase velocity which is quadratic in the wave vector **k**, and in the presence of fourth order spatial derivatives of the displacement field in the wave equation. We examine the unfolding under weak spatial dispersion of wave arrivals in the point force Green's functions of anisotropic solids. Specific attention is given to propagation in generic directions associated with elliptic or hyperbolic points on the acoustic slowness surface, i.e., points where the principal curvatures are respectively both of the same sign or opposite in sign. Acoustic axes and caustic directions fall outside the scope of this paper. In the response to a suddenly applied point force in the absence of dispersion, the wave arrival for an elliptic point normally takes the form of a step function (discontinuity), but in certain cases, usually pertaining to high symmetry directions, it can take the form of a ramp function (kink). The arrival for a hyperbolic point takes the form of a logarithmic singularity or, where symmetry intervenes, a softer logarithmic singularity. The first three of these types of arrival are conspicuous features in Fig. 1, which depicts a computed Green's function for propagation in the [110] direction in a copper crystal. The arrivals in the response to an impulsive force are the time derivative of the results we present in this paper, which pertain to a suddenly applied force.

The issues dealt with here are of relevance in a number of areas, including the topical subject of picosecond laser gen-

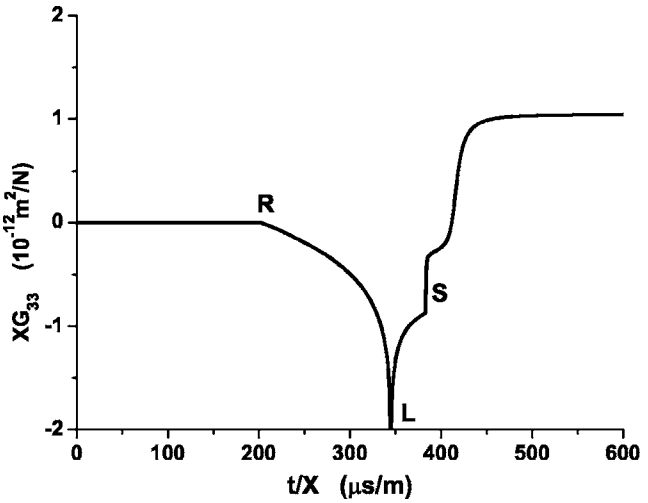

FIG. 1. Green's function for a copper crystal, for force and response in the [001] direction and observation point, **X**, in the [110] direction. *R* denotes the longitudinal wave arrival, which takes the form of a ramp function. The fast transverse (FT) sheet of the slowness surface is saddle shaped near the (001) plane, and as a result, the first FT arrival takes the form of the logarithmic singularity denoted *L*. There is a second FT arrival, actually two coincident arrivals, which takes the form of a step function denoted *S*, and derives from "oblique" modes associated with convex portions of the slowness surface. The slow transverse arrival lies out of range at 617 μs/m, and is a barely perceptible feature for symmetry reasons and also because of the smallness of $1/\sqrt{\alpha\beta}$, where $\alpha\beta$ is the Gaussian curvature of the slowness surface (see the discussion later).

erated ultrasound,[9] and they also bear on transient wave propagation in waveguides such as rods,[10] wires,[11] and plates.[5,12] The latter are subject to geometric dispersion, in which the natural length scale is the diameter or thickness, h. The primary concern of this paper is with the universal dynamical behavior of anisotropic solids under the first onset of spatial dispersion, i.e., the response of these solids to force distributions whose spatial and temporal frequency spectra are confined to the domain of weak spatial dispersion. In what follows, where we will loosely refer to a point or δ function $\delta(x)$ force, what is meant is a force of integrated magnitude unity, which is distributed over a region small compared to the distance X to the observation point, but nevertheless large compared to the natural length scale l. Likewise, where we will refer to a suddenly applied force, we imply a unit force with rise time small compared with X/v, where v is the sound speed, but large compared to l/v. Our point of departure in this paper is an earlier paper by one of the authors,[6] which describes the unfolding under spatial dispersion of wave arrivals in isotropic solids.

II. GENERAL FORMULATION

For centrosymmetric anisotropic solids, the first onset of spatial dispersion as the wavelength approaches the natural lenth scale, l, of the medium expresses itself through the presence of fourth order derivatives of the displacement field in the wave equation[6,13–15]

$$\rho\frac{\partial^2 u_p}{\partial t^2} = C_{pjql}\frac{\partial^2 u_q}{\partial X_j \partial X_l} + E_{pjqlmn}\frac{\partial^4 u_q}{\partial X_l \partial X_m \partial X_n \partial X_j}. \tag{1}$$

Here ρ is the mass density, and C_{pjql} and E_{pjqlmn} are material's tensors, respectively the normal and dispersive elastic constants. Equation (1) admits plane wave solutions of the form

$$u_p = U_p \exp i(\mathbf{k}\cdot\mathbf{X} - \omega t), \tag{2}$$

with the polarization vector, $\mathbf{U}=(U_p)$, wave vector, $\mathbf{k}=(k_p)$, wave normal, $\mathbf{n}=\mathbf{k}/k$, angular frequency, ω, and phase velocity, $v=\omega/k$, being related by the linear equations

$$\{(C_{pjql} - k^2 E_{pjqlmn} n_m n_n) n_l n_j - \rho v^2 \delta_{pq}\} U_q = 0. \tag{3}$$

For given $\mathbf{k}$, the solution of Eq. (3) yields three phase velocities, $v_{\mathbf{k}N}=\omega_{\mathbf{k}N}/k$; $N=1,2,3$, and associated polarization vectors, $\mathbf{U}^{\mathbf{k}N}=(U_p^{\mathbf{k}N})$, corresponding to a quasilongitudinal and two quasitransverse modes.

In this paper we treat dispersion as a perturbative effect on the wave equation, and to lowest order, this yields a correction to the phase velocity which is quadratic in k, i.e.

$$v_{\mathbf{k}N} = v_{\mathbf{n}N}(1 - \gamma_{\mathbf{n}N}k^2), \tag{4}$$

where the dispersion coefficient

$$\gamma_{\mathbf{n}N} = \frac{E_{pjqlmn} n_l n_j n_m n_n U_p^{\mathbf{n}N} U_q^{\mathbf{n}N}}{2\rho v_{\mathbf{n}N}^2}, \tag{5}$$

and $v_{\mathbf{n}N}$ and $\mathbf{U}^{\mathbf{n}N}$ are the limiting values of $v_{\mathbf{k}N}$ and $\mathbf{U}^{\mathbf{k}N}$ respectively, in the long wavelength $k\to 0$ limit. Equation (5) is obtained by first order perturbation theory, exploiting the symmetry with respect to interchange of p and q displayed by $C_{pjql}n_j n_l$ and $E_{pjqlmn}n_l n_j n_m n_n$, and the orthonormality of the $\mathbf{U}^{\mathbf{n}N}$ and the changes to the $\mathbf{U}^{\mathbf{k}N}$ under perturbation that this implies. The dispersion coefficient, $\gamma_{\mathbf{n}N}$, while thus depending on branch and direction, is in order of magnitude equal to $(l/2\pi)^2$. The condition of weak dispersion may be expressed as $\gamma_{\mathbf{n}N}k^2 \ll 1$, or equivalently $l \ll \lambda$. We will see that the small parameter for the theory below is $\eta = l/X$.

As shown in Ref. 6, the elastodynamic Green's function $G_{qp}(\mathbf{X},t)$, defined as the x_q'th component of the time-dependent displacement response at a point $\mathbf{X}$ in an infinite, dispersive anisotropic solid to a unit point force in the x_p direction acting at the origin $\mathbf{X}=0$, and having unit step function time dependence $\Theta(t)$, has the integral representation

$$G_{qp}(\mathbf{X},t) = \frac{A\Theta(t)}{\pi}\sum_{N=1}^{3}\int d^3k \exp(i\mathbf{k}\cdot\mathbf{X})\frac{\Lambda_{qp}^{\mathbf{k}N}}{(\omega_{\mathbf{k}N})^2} \times[1-\cos(\omega_{\mathbf{k}N}t)], \tag{6}$$

where

$$A = \frac{1}{8\pi^2\rho}. \tag{7}$$

This result is arrived at by a process involving Fourier transforming the differential equation for $G_{qp}(\mathbf{X},t)$, solving the resulting algebraic equation, and in the inverse transformation, integrating over frequency. Dispersion is taken account of in the cosine term

$$\cos(\omega_{\mathbf{k}j}t) = \cos[kv_{\mathbf{n}N}(1-\gamma_{\mathbf{n}N}k^2)t], \tag{8}$$

which, together with $\exp(i\mathbf{k}\cdot\mathbf{X})$ are the most rapidly varying terms in the integrand, but the more slowly varying factor $\Lambda_{qp}^{\mathbf{k}N}/(\omega_{\mathbf{k}N})^2$ is approximated by its dispersionless limit,

$$\Lambda_{qp}^{\mathbf{n}N}/(kv_{\mathbf{n}N})^2, \text{ where}$$

$$\Lambda_{qp}^{\mathbf{n}N} = U_q^{\mathbf{n}N}U_p^{\mathbf{n}N}. \tag{9}$$

In performing the integration with respect to $\mathbf{k}$, it is convenient to orient the k_3 axis in the direction of $\mathbf{X}$, and transform to spherical polar coordinates (k,θ,ϕ), in terms of which $\mathbf{k}\cdot\mathbf{X}=kX\cos\theta$. At this point, one has the choice of integrating either with respect to the angular coordinates first and then k, or the other way around. In our treatment of wave arrivals, we take the latter course in Secs. III and IV, integrating over k first, and then in the Appendix we briefly indicate how the same results can be arrived at by integrating over the angular coordinates first.

In the absence of dispersion, on integrating with respect to k, one obtains

$$G_{qp} = A\Theta(t)\sum_{N=1}^{3}\left\{\frac{1}{X}\int d\phi\frac{\Lambda_{qp}^{\mathbf{n}N}}{(v_{\mathbf{n}N})^2} - \int d\Omega\frac{\Lambda_{qp}^{\mathbf{n}N}}{(v_{\mathbf{n}N})^2} \times\delta(X\cos\theta - v_{\mathbf{n}N}t)\right\}. \tag{10}$$

The second term in (10) is a solid angular integral for $\mathbf{n}$, limited to the hemisphere centered on the observation direction. The first term in (10), which is an angular integral taken around the periphery of the hemisphere, is time independent, and represents the elastostatic Green's function for the medium. Equation (10), or results equivalent to it, has been obtained by a number of authors.[4,16–20] It is in a very convenient form for computations, and has been used in the calculation of Fig. 1.

In this paper we are specifically interested in the singular behavior of $G_{qp}(\mathbf{X},t)$ in the vicinity of wave arrivals, and how this unfolds under the influence of spatial dispersion, regardless of the particular component indices q and p and the branch N, so these indices are henceforth suppressed and the summation dropped. The time-independent terms in (6) and (10) are also dropped, and since t is implicitly positive, so is the factor $\Theta(t)$. The singular behavior for a particular arrival is thus given by an integral of the form

$$G = \frac{-A}{2\pi}\int dkd\Omega\Lambda s^2\left\{\exp i\left(\mathbf{k}\cdot\mathbf{X} - \frac{k}{s}(1-\gamma k^2)t\right) + \text{c.c.}\right\}, \tag{11}$$

where $\mathbf{s}=\mathbf{n}/v_{\mathbf{n}}$ is the phase slowness and c.c. denotes the complex conjugate of the previous term, which has arisen through exploiting the property $\omega_{-\mathbf{k}}=\omega_{\mathbf{k}}$. On replacing k by ks, we obtain

$$G = \frac{-A}{\pi}\int dkd\Omega\Lambda s^3\cos[k(\mathbf{s}\cdot\mathbf{X}-t)+\gamma s^2tk^3]. \tag{12}$$

In the above, the solid angular integral is over the unit sphere, and the integration limits for k are 0 and ∞. With the substitution

$$k = \frac{p\,\text{sgn}(\gamma)}{(3|\gamma|s^2t)^{1/3}}, \tag{13}$$

and integrating with respect to p, we obtain

$$G = -A\int d\Omega\frac{\Lambda s^3}{(3|\gamma|s^2t)^{1/3}}Ai\left(\frac{\text{sgn}(\gamma)}{(3|\gamma|s^2t)^{1/3}}(\mathbf{s}\cdot\mathbf{X}-t)\right), \tag{14}$$

where $\text{Ai}(z)=\frac{1}{\pi}\int_0^\infty dp\cos(zp+p^3/3)$ is the Airy function. The dispersionless classical continuum limit for G as $\gamma\to 0$, obtained using the identity

$$\lim_{\varepsilon\to 0}\frac{1}{\varepsilon}\text{Ai}\left(\frac{z}{\varepsilon}\right) = \delta(z), \tag{15}$$

is

$$G = -A\int d\Omega\Lambda s^3\delta(\mathbf{s}\cdot\mathbf{X}-t). \tag{16}$$

We regard (14) and (16) as integrals over the acoustic slowness surface, with $d\Omega$ denoting the solid angle subtended at the origin by a surface element.

A wave arrival is a singular feature in the Green's function at an observation point, $\mathbf{X}$, that arises in the integration over the neighbourhood of a point $\mathbf{s}_0$ on the slowness surface where the outward normal points in the direction of $\mathbf{X}$, rendering $\mathbf{s}\cdot\mathbf{X}$ is stationary. It is the high frequency Fourier components of the signal that propagate the wave arrival singularity, and these conform to the stationary phase approximation, with the outward normal being the ray direction. The singularity has arrival time $\mathbf{s}_0\cdot\mathbf{X}=t_0$ and propagates with group velocity $\mathbf{V}=\mathbf{X}/t_0$. To determine the singular form of the arrival and its unfolding, we perform the integrations in (16) and (14) in a local coordinate frame with s_3 oriented along the outward normal and s_1 and s_2 in the directions of principal curvature of the slowness surface at $\mathbf{s}_0$. Locally, the equation for the slowness surface can be approximated by

$$s_3 = -\frac{\alpha}{2}s_1^2 - \frac{\beta}{2}s_2^2, \tag{17}$$

where α and β are the principal curvatures, and $\alpha\beta$ is the Gaussian curvature of the slowness surface. In this paper we treat only generic points, where both curvatures and hence $\alpha\beta$ are finite. Points of vanishing Gaussian curvature map onto fold edges of the wave surface and caustics in the acoustic intensity, and will be the subject of a later paper. Also not discussed here are acoustic axes, i.e., points of degeneracy in the slowness surface, where $\alpha\beta$ is infinite or undefined. One distinguishes between elliptic points for which $\alpha\beta>0$ and the surface is either convex $(\alpha,\beta>0)$ or concave $(\alpha,\beta<0)$, and hyperbolic points for which $\alpha\beta<0$

and the surface is saddle shaped, with α and β opposite in sign.

In the local coordinate frame we have that

$$\mathbf{s}\cdot\mathbf{X}-t=\left[\mathbf{s}_0+\left(s_1,s_2,-\frac{\alpha}{2}s_1^2-\frac{\beta}{2}s_2^2\right)\right]\cdot\mathbf{X}-t$$
$$=-\left(\frac{\alpha}{2}s_1^2+\frac{\beta}{2}s_2^2\right)X-\tau, \tag{18}$$

where

$$\tau=t-t_0, \tag{19}$$

is time measured from the arrival. The solid angle $d\Omega$ corresponding to an area element ds_1ds_2 on the slowness surface, is given by

$$d\Omega=\frac{ds_1ds_2\cos(\chi)}{s_0^2}=\frac{ds_1ds_2}{s_0^3V}, \tag{20}$$

where χ is the angle between $\mathbf{s}_0$ and $\mathbf{X}$. Use has been made of the identity $\mathbf{s}_0\cdot\mathbf{V}=s_0V\cos(\chi)=1$ in (20). With this substitution, (14) and (16) become

$$G=\frac{-A\Lambda}{V\tau_0}\int ds_1ds_2\mathrm{Ai}\left(-\frac{\mathrm{sgn}(\gamma)}{\tau_0}\left[\left(\frac{\alpha}{2}s_1^2+\frac{\beta}{2}s_2^2\right)X+\tau\right]\right), \tag{21}$$

and

$$G=\frac{-A\Lambda}{V}\int ds_1ds_2\delta\left[\left(\frac{\alpha}{2}s_1^2+\frac{\beta}{2}s_2^2\right)X+\tau\right], \tag{22}$$

respectively, where

$$\tau_0=(3|\gamma|s_0^2t_0)^{1/3} \tag{23}$$

is the time scale for the unfolding of the wave arrival. In terms of the small parameter, $\eta=l/X$,

$$\tau_0=a\eta^{2/3}t_0, \tag{24}$$

where $a=0.42(\cos\chi)^{-2/3}$ is a numerical quantity of order unity.

In the next two sections, we treat respectively the wave-arrival singularities and their unfoldings for elliptic and hyperbolic points on the slowness surface, proceeding from (22) and (21), with the integration with respect to k having been performed first. In the Appendix we indicate how equivalent results can be arrived at by doing the integration with respect to s_1 and s_2 first.

III. ELLIPTIC POINTS ON SLOWNESS SURFACE

In the case of elliptic points where the slowness surface is either convex $(\alpha,\beta>0)$ or concave $(\alpha,\beta<0)$, we proceed with the integration of (21), by effecting the following changes of variables:

$$\frac{\alpha X}{2\tau_0}s_1^2=x^2, \tag{25}$$

$$\frac{\beta X}{2\tau_0}s_2^2=y^2, \tag{26}$$

$$\tau=T\tau_0, \tag{27}$$

where T is a dimensionless time. This yields

$$G=\frac{2\pi A\Lambda}{\sqrt{\alpha\beta}VX}I(T), \tag{28}$$

where

$$I(T)=-\frac{1}{\pi}\int dxdy\mathrm{Ai}\{-\mathrm{sgn}(\gamma)[\mathrm{sgn}(\alpha)(x^2+y^2)+T]\}. \tag{29}$$

A similar change of variables on (22) for the dispersionless limit yields the same result (28) except with $I(T)$ replaced by

$$I_0(T)=-\frac{1}{\pi}\int dxdy\delta[\mathrm{sgn}(\alpha)(x^2+y^2)+T]. \tag{30}$$

Changing to polar coordinates

$$x=r\cos\varphi,\quad x=r\sin\varphi, \tag{31}$$

and then to the variable

$$p=r^2, \tag{32}$$

the integration with respect to φ yields 2π, and we arrive at the following results for the singular behavior near the arrival

$$I(T)=-\int_{T\,\mathrm{sgn}(\alpha)}^{\infty}dp\mathrm{Ai}[-\mathrm{sgn}(\alpha)\mathrm{sgn}(\gamma)p], \tag{33}$$

and

$$I_0(T)=-\Theta[-\mathrm{sgn}(\alpha)T]. \tag{34}$$

For given τ, as $\gamma\to0$, $T=\tau/\tau_0\to\infty$ and (33) converges to (34).

In the dispersionless limit the arrival, as is well known,[4] thus takes the form of a discontinuity or step function, with magnitude equal to $2\pi A\Lambda/\sqrt{\alpha\beta}VX$. The smaller the Gaussian curvature $\alpha\beta$, the larger is the discontinuity and the acoustic energy it propagates. In the context of phonon transport, this is referred to as phonon focusing. Equations (28) and (33) represent the generalization of Eq. (21) of Ref. 6 for the unfolding of the step function arrival in an isotropic solid. The result there is obtained by setting $\alpha=\beta=V$, $\Lambda=1$, and $\mathrm{sgn}(\alpha)=1$ in (28) and (33). Thus, the functional form of the arrival and its unfolding for convex points on the slowness surface is unaffected by anisotropy, although its magnitude is. The step function arrival and its unfolding are depicted in Fig. 2 for the different combinations of signs of α and γ. The sign of α determines whether the step is positive or negative, and the sign of γ determines whether the ripples of the wave train follow $(\gamma>0)$ or precede $(\gamma<0)$ the undispersed arrival.

A. Behavior near to directions of zero spatial dispersion

For an anisotropic solid, there can in principle exist a one parameter manifold of directions (lines on the unit sphere)

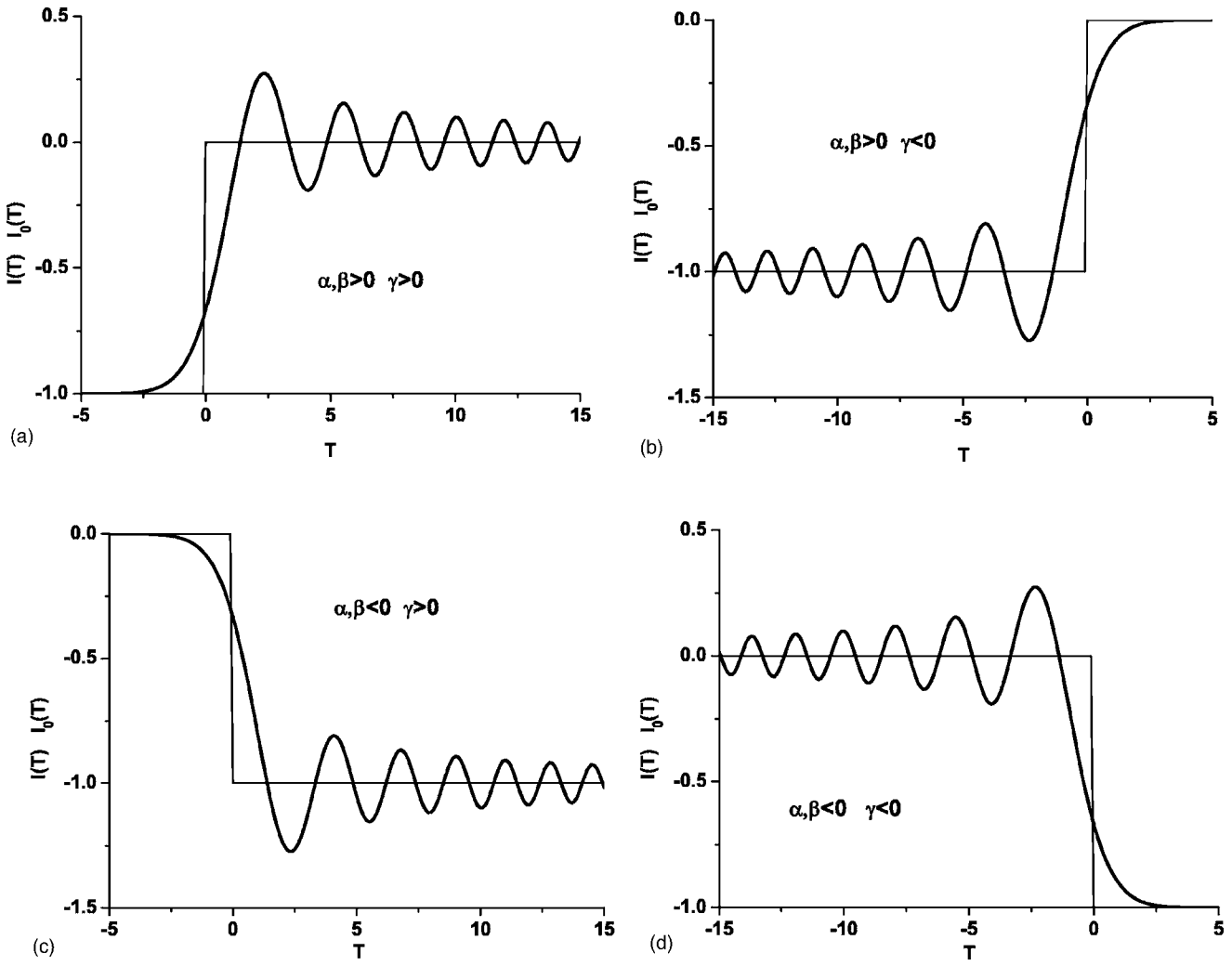

FIG. 2. The step function arrival $I_0(T)$ and its unfolding $I(T)$ (bold) under positive (a, c) and negative (b, d) spatial dispersion, and for convex (a, b) and concave (c, d) regions of the slowness surface.

separating regions of positive and negative γ. Nearby, γ will vary linearly with angular deviation ϕ from the manifold, and hence from (24) and (27)

$$T = b|\phi|^{-1/3}\tau, \tag{35}$$

where b is a constant. Expressed as a function of the time from arrival τ, the unfolding of the wave arrival is described by $I[b|\phi|^{-1/3}\tau, \mathrm{sgn}(\phi), \mathrm{sgn}(\alpha)]$, from which it follows that the temporal spacing of the ripples tends to zero as $|\phi|^{1/3}$ when $\phi \to 0$, at which point they undergo a reversal between following and preceding. This behavior is depicted in Fig. 3, which portrays $I[b|\phi|^{-1/3}\tau, \mathrm{sgn}(\phi), \mathrm{sgn}(\alpha)]$ as a gray scale. Near to the crossover, where γ is very small, higher order corrections in the dispersion relation will become important. A more accurate representation of the dispersion relation in the form

$$\omega = vk(1 - \gamma k^2 - \zeta k^4), \tag{36}$$

would yield a smooth transition between following and preceding ripples.

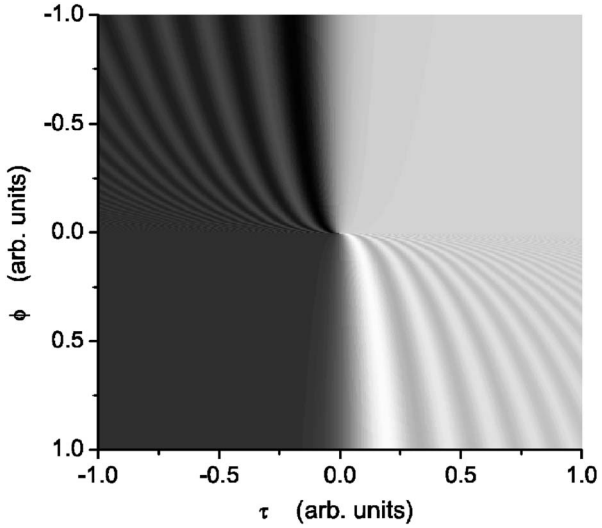

FIG. 3. Gray scale representation of the variation with ϕ of the unfolding of the step function arrival, showing reversal of the location of the ripples as ϕ changes sign.

B. Ramp arrival and its unfolding in directions for which $\Lambda(\mathbf{s})=0$

Ramp arrivals are conditioned by the vanishing of $\Lambda(\mathbf{s})$, and are thus usually to be found in symmetry directions, although this is not a requirement for their existence. We consider a medium possessing a mirror symmetry plane, which we orient the [010] axis normal to, and a generic observation point $\mathbf{X}$, which we take to locate the [001] direction in this plane. On symmetry grounds, $G_{12}(\mathbf{X})=G_{21}(\mathbf{X})=G_{32}(\mathbf{X})=G_{23}(\mathbf{X})=0$. Further, the three sheets of the slowness surface intersect this symmetry plane normally, except at isolated points of conical degeneracy, which lie outside the scope of this paper. One of these lines of intersection is an ellipse, and pertains to a pure transverse (T) mode with polarization in the [010] direction, and which is uncoupled from the other two modes. There is a single point $\mathbf{s}_0$ on this ellipse whose associated ray vector points in the observation direction. The directions and values of the principal curvatures of the slowness surface at $\mathbf{s}_0$ are [100] for α and [010] for β, and both curvatures are positive. On the ellipse, $\Lambda_{11}=\Lambda_{33}=\Lambda_{13}=\Lambda_{31}=0$, and as a result the T arrival in the corresponding components of the G_{qp} tensor is not a discontinuity, but a softer singular form (this is not the case for G_{22}, since Λ_{22} is nonvanishing). We obtain this softer singularity by considering the variation of Λ out of the plane, which takes the form $\Lambda=es_2^2$, where e is a positive constant. In the vicinity of the T arrival, G is thus given by

$$G=\frac{-Ae}{V\tau_0}\int ds_1 ds_2 s_2^2 \mathrm{Ai}\left\{-a\ \mathrm{sgn}(\gamma)\left[\left(\frac{\alpha}{2}s_1^2+\frac{\beta}{2}s_2^2\right)X+\tau\right]\right\}. \tag{37}$$

On implementing the change of variables (25)–(27), Eq. (37) becomes

$$G=\frac{2\pi Ae\tau_0}{\sqrt{\alpha\beta^3}VX^2}L(T), \tag{38}$$

where

$$L(T)=-\int_T^\infty dp(p-T)\mathrm{Ai}[-\mathrm{sgn}(\gamma)p]. \tag{39}$$

Equation (38) applies in the dispersionless limit, with $L(T)$ replaced by

$$L_0(T)=T\Theta(-T). \tag{40}$$

Equations (38) and (39) represent the generalization of Eq. (24) of Ref. 6 for the unfolding of the ramp function arrival in an isotropic solid. Thus, the ramp arrival and its unfolding is unaffected by anisotropy, although its magnitude is. The ramp function arrival and its unfolding are depicted in Fig. 4 for positive and negative γ.

IV. HYPERBOLIC POINTS ON SLOWNESS SURFACE

In the case of hyperbolic points on the slowness surface, the principal curvatures α and β are opposite in sign. G is now given by

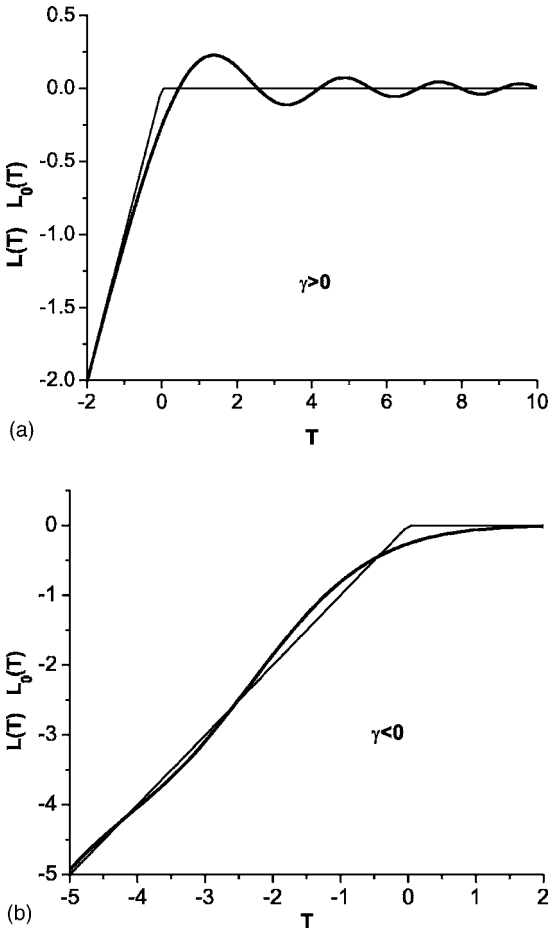

FIG. 4. The ramp function arrival $L_0(T)$ and its unfolding $L(T)$ (bold) under positive (a) and negative (b) spatial dispersion.

$$G=\frac{2A\Lambda}{\sqrt{-\alpha\beta}VX}K(T), \tag{41}$$

where T as before is given by (27), and

$$K(T)=-\int dxdy\mathrm{Ai}[x^2-y^2-\mathrm{sgn}(\gamma)T]. \tag{42}$$

The dispersionless limit yields the same result (41) except with $K(T)$ replaced by

$$K_0(T)=-\int dxdy\,\delta(x^2-y^2-T). \tag{43}$$

Since $\delta(-z)=\delta(z)$, it follows that $K_0(-T)=K_0(T)$. In contrast, the Airy function does not possess inversional symmetry, and so $K(T)$ is not a symmetric function of T.

Both the integrals (42) and (43) diverge logarithmically when the limits for x and y are taken to be infinity, and it is necessary to impose a large but finite cutoff. This is not simply a mathematical expedient, we are dealing with a local approximation to the equation of the slowness surface, which is just not applicable to large values of x and y. Fortunately the position of the cutoff merely determines an additive constant, and has no influence whatsoever on the singular behavior at the arrival.

To proceed with the integration of (42) and (43), we transform to hyperbolic coordinates

$$u = 2xy, \tag{44}$$

$$v = x^2 - y^2, \tag{45}$$

the Jacobian for the transformation being

$$|J| = \left| \frac{\partial(x,y)}{\partial(u,v)} \right| = \frac{1}{4\sqrt{v^2+u^2}}. \tag{46}$$

We limit the integration to the first and third quadrants in which $u>0$ (all four quadrants contribute equally to the integral), and the result is

$$K(T) = -\frac{1}{2}\int_{-c}^{c} dv \mathrm{Ai}[v - \mathrm{sgn}(\gamma)T] \int_{0}^{c} \frac{du}{\sqrt{v^2+u^2}}. \tag{47}$$

The major contribution to the double integral comes from the region where the argument of the Airy function is of order unity, and this function is neither very small nor oscillating rapidly. It is sufficient therefore to take the cutoff c appreciably larger than $|T|$ but nevertheless finite. Performing the integration with respect to u one obtains

$$K(T) = \frac{1}{2}\int_{-c}^{c} dv \mathrm{Ai}[v - \mathrm{sgn}(\gamma)T] \ln\left(\frac{v^2}{4c^2}\right). \tag{48}$$

where $\ln = \ln_e$ is the natural logarithm.The same steps applied to (43) yield

$$K_0(T) = \frac{1}{2}\int_{-c}^{c} dv\, \delta(v-T) \ln\left(\frac{v^2}{4c^2}\right) = \ln(|T|) - \ln(2c). \tag{49}$$

The logarithmic divergence for the undispersed arrival had been noted by several authors in the past.[4,16–19,21] Its unfolding under dispersion is obtained by carrying out the integration in (48) numerically.

Because v an c appear squared in the logarithm factor in (48), it is convenient to take the lower limit as 0, and cast (48) in the form

$$K(T) = \int_{0}^{c} dv \{\mathrm{Ai}[-v - \mathrm{sgn}(\gamma)T] + \mathrm{Ai}[v - \mathrm{sgn}(\gamma)T]\} \ln\left(\frac{v}{2c}\right). \tag{50}$$

Note that c appears both in the integrand and as the upper limit of integration. In the numerical evaluation of this integral, in order to avoid the appearance of spurious high frequency oscillations in the results, one replaces the sharp upper limit with a smooth cutoff, which we have implemented with the windowing function

$$f(v) = \frac{1}{2}\left[\cos\left(\frac{\pi v^2}{2c^2}\right) + 1\right]. \tag{51}$$

This function is close to unity for $v<0.5c$ and then drops off fairly rapidly near $v=c$ and reaches zero at $\sqrt{2}c$, which we take to be the upper limit of integration. Figure 5 shows the results of calculation of $K(T)$ compared with $K_0(T)$ for γ positive and $c=60/\sqrt{2}$. For γ negative, $K(T)$ is the mirror image around $T=0$, of that in Fig. 5.

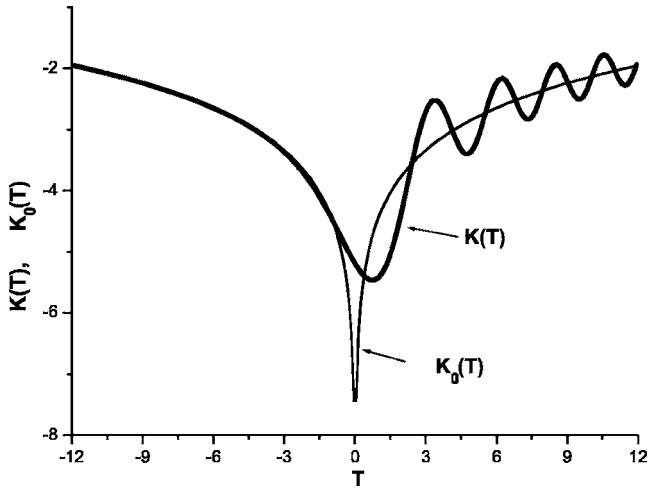

FIG. 5. $K(T)$ compared with $K_0(T)$ for γ positive and $c=60/\sqrt{2}$.

For $T<0$, $K(T)$ lies very close to $K_0(T)$, the reason being that in this limit only the one Airy term $\mathrm{Ai}(-v-T)$ contributes significantly to the integral, doing so mainly where $-v-T\approx 0$. Therefore, $\mathrm{Ai}(-v-T)$ can be replaced to a good approximation by $\delta(-v-T)$, yielding (49). For $T>0$, both Airy terms contribute to the integral as shown in Fig. 6, in which K_- and K_+ represent the contributions of $\mathrm{Ai}(-v-T)$ and $\mathrm{Ai}(-v-T)$ respectively to $K(T)$. The ripples for the two contributions are of approximately the same frequency, but are in antiphase, and there is partial cancellation when they are combined into $K(T)$. The oscillations for K_- are superimposed on a logarithmic background, which is retained when the two contributions are combined. For $T>0$, one would expect the oscillations to die out, and $K(T)$ to approach $K_0(T)$. This is precisely what happens, as shown in Fig. 7, which reveals that $K(T)-K_0(T)$ in fact tends to $-\mathrm{Ai}(-T)$ for large $|T|$.

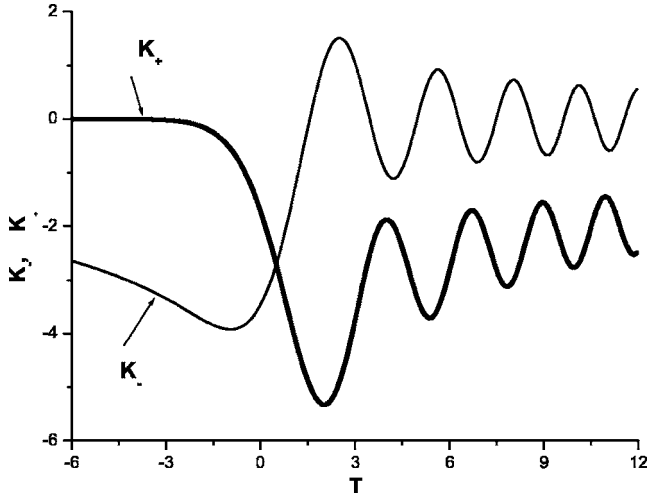

FIG. 6. The contributions K_- and K_+ to $K(T)$.

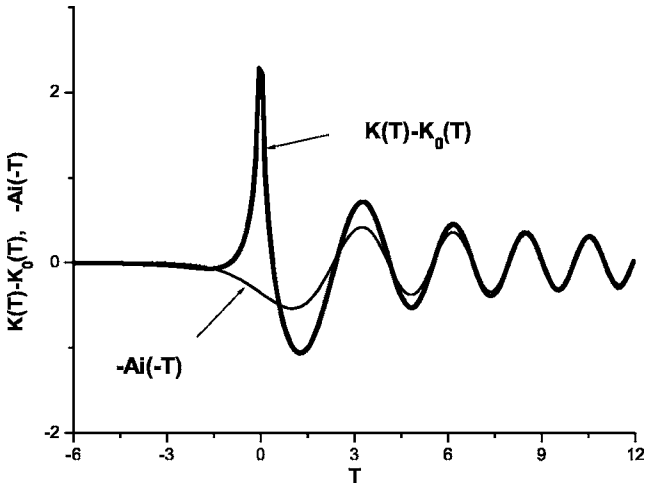

FIG. 7. $K(T)-K_0(T)$ compared with $-\mathrm{Ai}(-T)$.

A. Near directions of zero spatial dispersion

Near directions of zero spatial dispersion, similar behavior is predicted to that described in Sec. III A, with the ripples becoming more closely spaced as $\phi \to 0$, and then undergoing reversal between following and preceding. Again, taking account of higher order terms in the dispersion relation would have the effect of smoothing out this transition.

B. Soft logarithmic arrival and its unfolding in directions for which $\Lambda(\mathbf{s})=0$

Soft logarithmic arrivals are conditioned by the vanishing of $\Lambda(\mathbf{s})$ for hyperbolic points on the slowness surface. Our treatment of this arrival parallels that of the ramp arrival, but with the slowness surface curvature transverse to the symmetry plane being negative. Thus, setting $\Lambda=es_2^2$, and implementing the same changes of variables as before, we obtain

$$G = \frac{4Ae\tau_0}{\sqrt{-\alpha\beta^3}VX^2} M(T), \tag{52}$$

where

$$M(T) = -\int dxdyy^2 \mathrm{Ai}[x^2 - y^2 - \mathrm{sgn}(\gamma)T]. \tag{53}$$

Transforming to hyperbolic coordinates and integrating with respect to u, one obtains

$$M(T) = -\frac{1}{4}\int_{-c}^{c} dv \mathrm{Ai}\{-\mathrm{sgn}(\gamma)[v+T]\}\left[c + v\ln\left(\frac{v^2}{4c^2}\right)\right]. \tag{54}$$

The same steps applied in the nondispersive limit yield

$$M(T) = \frac{T}{2}\ln\left(\frac{|T|}{2c}\right) - \frac{c}{4}. \tag{55}$$

This arrival thus propagates a soft singularity, which is difficult to discern in a graphical plot. In the response to an impulsive force, the arrival is given by the time derivatives of (54) and (55), and is more pronounced.

V. CONDITIONS FOR THE OBSERVATION OF QUASIARRIVALS

In measuring time domain dynamic response functions, by whatever means, there are practical constraints affecting the observability of wave-arrival unfoldings. A method that is particularly suited to measuring the small scale features of quasiarrivals is the picosecond laser pump-probe method.[9] For a subpicosecond laser pulse, the duration of the resulting transient forces is small compared to the characteristic time τ_0 defined by (24), for any plausible scenario, and so this time spread is not a significant source of broadening in the acoustic signal. The more important consideration is the limitation imposed by the finite size of the regions in which the generation and detection of the acoustic wave takes place.

The experimental situation we envisage is of a slab-shaped crystal, which for calculational purposes we will take to be of thickness $h=5$ nm, through which propagation of the wave to be observed takes place. Assuming the wave speed to be $V=5000$ m/s and the crystal lattice constant to be $l=0.5$ nm, and setting $|\gamma|=(l/2\pi)^2$ and $\cos\chi=1$, it follows that the spatial interval between the first two fringes in the quasiarrival is equal to $3.8\tau_0 V=3.8V(3l^2h/4\pi^2)^{1/3}=173$ nm. The interaction of the pump and probe laser beams with the sound takes place in aluminium coatings of between 10 and 20 nm in thickness on the opposite faces of the crystal. This thickness is much smaller than the aforementioned ripple separation, and so also is not a significant source of broadening in the acoustic signal. The surface regions illuminated by the lasers are, on the other hand, several microns or even tens of microns in diameter, greatly exceeding both the film thickness and the ripple separation, although still small compared with the sample thickness, and this is of great importance. Because of the finite source and detection volumes, the effective source-detector distance $\mathbf{X}$ is distributed around a mean value $\mathbf{X}_0=\mathbf{V}_0 t$, and the observed signal will be the convolution of the Green's function $G(\mathbf{X},t)$ with this distribution function. The small variation of $\mathbf{X}$ normal to the sample's surface, as we have seen, has a negligible effect on the observed signal, but not so the broad distribution of values of $\mathbf{X}$ parallel to the sample's surface. This will cause the washing out of the ripples in the quasiarrival through phase cancellation, except at points $\mathbf{X}_0$ where the acoustic wave surface, along which the three dimensional pattern of ripples is aligned, is parallel to the sample's surface. Normal to the wave surface is the slowness vector $\mathbf{s}_0$, implying that the observed signal is derived mainly from partial waves with $\mathbf{k}$'s normal to the sample's surface, as one might expect. To observe the unfolded wave arrival associated with a specific point on the wave surface will thus require cutting the sample's surfaces parallel to the wave surface at that point.

There is an upper bound to the width d of the distribution function for $\mathbf{X}$, i.e., the diameter of the laser beams, beyond which washing out of the ripples occurs, even for the aforementioned special directions, and this derives from the curvature of the wave surface. Assuming a roughly spherical wave surface of radius equal to the sample thickness h, in order for there not to be significant cancelling out of the ripples in the convolution integral, $d^2/8h$ should be smaller

than $3.8\tau_0 V$, and hence $d<83$ μm, which condition should be easily met in practice.

There are two possible avenues for overcoming the restrictions described above on the directions in which quasiarrivals can be observed. One is to dramatically reduce the lateral dimensions of the source and detection volumes, say by irradiating metallic "quantum dots" or other nanostructures of size $d<3.8\tau_0 V=173$ nm, rather than continuous films. There has in fact already been progress in achieving nanoscale imaging with acoustic frequencies approaching 1 GHz in laser pump-probe experiments.[22,23] These developments might provide the means for observing the craters produced by the "Coulomb explosions" that take place when slowly moving highly charged ions approach a solid surface, and even possibly the shock waves generated during the explosions.[24] The second route is to carry out measurements on systems such as fiber composites or phononic crystals, etc., for which the natural scale of length is much greater than interatomic distances. Colloidal crystals[25] and Ni-based superalloys[26] displaying rafting structures are two examples of solids for which $l\approx 1$ μm. Appropriate scaling of the numerical estimates above yields $3.8\tau_0 V=27.5$ μm in this case. It should not be overly difficult to confine the source-detector distribution within these bounds in all three directions.

In order to observe arrivals associated with hyperbolic and concave portions of the slowness surface, there is a second condition that has to be met. For moderately anisotropic solids there are some directions in which there are only three arrivals, all associated with convex portions of the slowness surface, and the group velocity (ray) surface is unfolded. The quasiarrivals here tend to be well separated and resolving them is unlikely to present a problem. The challenge comes in resolving less well separated quasiarrivals associated with folded portions of the ray surface (see Fig. 8, which pertains to silicon). It is only in these folded regions that one encounters arrivals associated with hyperbolic and concave points on the slowness surface. Si can be regarded as a fairly typical moderately anisotropic solid, and we see that group velocities within folded regions of the ray surface, in this case, tend to differ in the order of 1%, and hence the spatial separation between successive wave arrivals for a travel distance h, is of order $h/100$. This distance should be greater than about 5 times the initial ripple interval to observe reasonably well separated quasiarrivals. This implies that $h>1900\tau_0 V$, which comes out to 0.086 mm for a crystal, and 1.37 cm for a medium for which $l\approx 1$ μm. Neither figure is unreasonably large.

VI. BEYOND THE REGIME OF WEAK SPATIAL DISPERSION

The results of this paper are relevant only to force distributions fulfilling the conditions of weak spatial dispersion, where $\omega\approx v_0 k(1-\gamma k^2)$; $|\gamma|k^2<1$. Within this regime, one observes universal behavior in the unfolding of wave-arrival singularities into pseudoarrivals. In some cases, such as for directions in which $\gamma=0$, it is useful to consider higher powers of k in the dispersion relation, but in general this is a course of diminishing returns. To go much beyond the limits

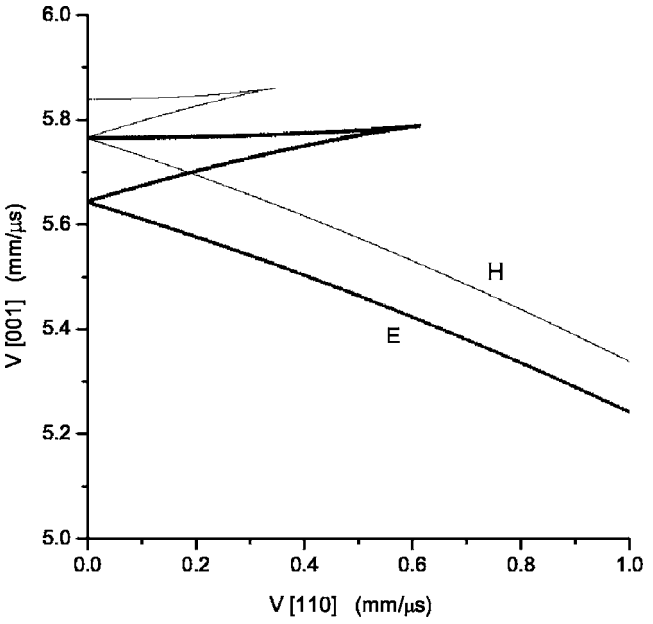

FIG. 8. $(1\bar{1}0)$ section of the folded region of the group velocity surface of silicon near the [001] axis. *H* and *E* denote respectively wave sheets associated with hyperbolic and convex elliptic points on the slowness surface.

of weak dispersion, is to encounter wavelengths comparable to or smaller than l. In this situation there is limited scope for a generalized approach, and one needs rather to examine the micromechanics of each particular system, whether it be a crystal lattice, a layered solid of some sort, a phononic crystal, or whatever. In most cases there will be higher order bands and frequency band gaps to contend with. Many different outcomes are possible, ranging to the limiting case of pulses which are extremely short compared to l, that will undergo frequent scattering and consequently propagate diffusely. In this paper we have not attemped to engage with this multitude of possibilities that lies beyond the domain of weak spatial dispersion.

ACKNOWLEDGMENTS

This research was funded by a grant from the EPSRC. A.G.E. gratefully acknowledges the hospitality of Brunel University, where most of this work was carried out, and thanks E. Sideras-Haddad and K. Jakata for drawing his attention to recent nanoscale materials developments.

APPENDIX. INTEGRATING OVER s_1 AND s_2 FIRST

The results of Secs. III and IV can alternatively be established by carrying out the integration over s_1 and s_2 in (11) before that of k. We briefly sketch how this is may be done. On replacing k by ks, and making the substitutions (18)–(20), one obtains

$$G = \frac{-A\Lambda}{2\pi V}\int_0^\infty dk \int ds_1 ds_2 \times \left\{ \exp(ik)\left[-\left(\frac{\alpha}{2}s_1^2 + \frac{\beta}{2}s_2^2\right) - \tau + k^2\gamma s_0^2 t_0 \right] + \text{c.c.} \right\}. \tag{A1}$$

On making the further substitutions

$$\frac{Xk|\alpha|}{2}s_1^2 = x^2, \tag{A2}$$

$$\frac{Xk|\beta|}{2}s_2^2 = y^2, \tag{A3}$$

and integrating with respect to x and y, one obtains

$$G = \frac{-A\Lambda}{\sqrt{|\alpha\beta|}VX}\int_0^\infty \frac{dk}{k}\left\{ \exp(ik)(-\tau + k^2\gamma s_0^2 t_0)\exp\frac{-i\pi}{4}[\text{sgn}(\alpha) + \text{sgn}(\beta)] + \text{c.c.} \right\}. \tag{A4}$$

For elliptic points on the slowness surface, (A4) simplifies to

$$G = \frac{2A\Lambda\ \text{sgn}(\alpha)}{\sqrt{\alpha\beta}VX}\int_0^\infty \frac{dk}{k}\sin(k\tau - k^3\gamma s_0^2 t_0), \tag{A5}$$

while for hyperbolic points it simplifies to

$$G = \frac{-2A\Lambda}{\sqrt{-\alpha\beta}VX}\int_\varepsilon^\infty \frac{dk}{k}\cos(k\tau - k^3\gamma s_0^2 t_0). \tag{A6}$$

Again, for hyperbolic points, a cutoff must be imposed to avoid divergence. In this case, however, it applies to the lower limit, which is taken to have a small but positive value, ε, rather than zero.

In the dispersionless limit $\gamma \to 0$, integration of (A5) for elliptic points yields

$$G = \frac{\pi A\Lambda\ \text{sgn}(\alpha)\text{sgn}(\tau)}{\sqrt{\alpha\beta}VX}, \tag{A7}$$

which differs from (28) and (34) only by an additive constant, while for hyperbolic points, (A6) yields

$$G = \frac{2A\Lambda[\ln(|\tau|) + \ln(\varepsilon) + 0.577]}{\sqrt{-\alpha\beta}VX}, \tag{A8}$$

which is consistent with (41) and (49).

A way of recovering (28) and (33) for the unfolding of the step function arrival, is to differentiate (A5) with respect to τ, and change the integration variable to $\xi = \tau_0 k$, yielding

$$\frac{dG}{d\tau} = \frac{2\pi A\Lambda\ \text{sgn}(\alpha)}{\sqrt{\alpha\beta}VX\tau_0}H(T), \tag{A9}$$

where

$$H(T) = \frac{1}{\pi}\int_0^\infty d\xi \cos[\xi T - \xi^3\ \text{sgn}(\gamma)/3] = \text{Ai}[-T\ \text{sgn}(\gamma)], \tag{A10}$$

and, as before, $T = \tau/\tau_0$. This is the response to an impulsive point force. Integration with respect to τ now yields (28) and (33). A similar approach can be taken to obtain the unfolding of the logarithmic arrival.

*Electronic address: everya@physics.wits.ac.za

[1] K. Aki and P. G. Richards, *Quantitative Seismology* (University Science Books, Sausalito, CA, 2002), 2nd edition.
[2] A. Ben-Menahem and S. J. Singh, *Seismic Waves and Sources* (Dover, Mineola, 1981), 2nd edition.
[3] J. D. Achenbach, *Wave Propagation in Elastic Solids* (North Holland, Amsterdam, 1993).
[4] A. G. Every and K. Y. Kim, J. Acoust. Soc. Am. **95**, 2505 (1994).
[5] J. D. Kaplunov, L. Yu. Kossovich, and E. V. Nolde, *Dynamics of Thin Walled Elastic Bodies* (Academic Press, San-Diego, 1998).
[6] A. G. Every, Phys. Rev. B **72**, 104302 (2005).
[7] R. M. Christensen, *Mechanics of Composite Media* (Wiley, New York, 1979).
[8] M. Elices and F Garcia-Moliner, in *Physical Acoustics*, edited by W. P. Mason, Volume V (Academic, New York, 1968), Chap. 4.
[9] H.-Y. Hao and H. J. Maris, Phys. Rev. B **63**, 224301 (2001).
[10] C. Bescond (private communication).
[11] E. Ducasse, J. Acoust. Soc. Am. **118**, 1776 (2005).
[12] J. D. Kaplunov and A. V. Pichugin, J. Mech. Phys. Solids **53**, 1079 (2005).
[13] D. P. DiVincenzo, Phys. Rev. B **34**, 5450 (1986).
[14] *Mechanics of Generalized Continua*, edited by E. Kröner (Springer, Berlin, 1968).
[15] R. Lakes, in *Continuum Models for Materials with Microstructure*, edited by H. Muhlhaus (Wiley, New York, 1995), Chap. 1.
[16] V. T. Buchwald, Proc. R. Soc. London **253**, 563 (1959).
[17] R. Burridge, Q. J. Mech. Appl. Math. **20**, 41 (1967).
[18] N. Cameron and G. Eason, Q. J. Mech. Appl. Math. **20**, 23 (1967).
[19] C.-Y. Wang and J. D. Achenbach, Wave Motion **18**, 273 (1993).
[20] V. K. Tewary, Phys. Rev. B **51**, 15695 (1995).
[21] R. G. Payton, *Elastic Wave Propagation in Transversely Isotropic Media* (Martinus Nijhoff, The Hague, 1983).
[22] B. C. Daly, N. C. R. Holme, T. Buma, C. Branciard, T. B. Norris, D. M. Tennant, J. A. Taylor, J. E. Bower, and S. Pau, Appl. Phys. Lett. **84**, 5180 (2004).
[23] K.-H. Lin, C.-T. Yu, S.-Z. Sun, H.-P. Chen, C.-C. Pan, J.-I. Chyi, S.-W. Wang, P.-C. Li, and C.-K. Sun, Appl. Phys. Lett. **89**, 043106 (2006).
[24] H.-P. Cheng and J. D. Gillaspy, Phys. Rev. B **55**, 2628 (1997).
[25] P. Schall, I. Cohen, D. A. Weitz, and F. Spaepen, Nature (London) **440**, 319 (2006).
[26] See papers on $L1_2$ ordered alloys in *Dislocations in Solids*, edited by F. R. N. Nabarro and M. S. Duesbery (North-Holland, Amsterdam, 1996).